JOURNAL OF GUIDANCE, CONTROL, AND DYNAMICS
Vol. 23, No. 6, November–December 2000

Quantitative Cross-Feed and Feedback Design of Helicopter in near Hover Flight

Ukpai I. Ukpai* and O. D. I. Nwokah†
Southern Methodist University, Dallas, Texas 75275-0337
and
Edward Boje‡
University of Natal, Durban 4041, South Africa

This paper examines the use of quantitative cross-feed design followed by diagonal feedback design to decouple, stabilize, and improve handling qualities of the UH-60 Black Hawk helicopter near hover. The flight configurations used were classified according to the likelihood of their occurrence in practice, and this allows the performance for usual cases to be improved by a tradeoff with reduced but still quantitative performance for less usual operating conditions. The design is based on a set of linear models obtained from a nonlinear model with six-degree-of-freedom rigid fuselage with rigid rotor blades, each with a flap and lag degree of freedom. The Perron root of the interaction matrix is used as a measure of the level of interaction of uncertain multivariable plants, and the cross-feed design seeks to reduce the interaction index before quantitative design of a diagonal controller matrix is attempted. If the interaction index can be made to be less than unity by the design, stability of the diagonal-loop design guarantees stability of the closed-loop multivariable system. Performance is evaluated against some of the requirements of the Aeronautical Design Standard, ADS-33D-PRF, for near hover flight.

Nomenclature

$\boldsymbol{A}$	=	open-loop dynamics matrix
a_{ij}	=	upper limit of response specification for element i, j
$\boldsymbol{B}$	=	input distribution matrix
b_{ij}	=	lower limit of response specification for element i, j
$\boldsymbol{C}$	=	measurement distribution matrix, state vector
$\boldsymbol{D}$	=	measurement distribution matrix, control vector
$\boldsymbol{F}$, (f_{ij})	=	prefilter matrix (element i, j)
$\boldsymbol{G}$, (g_{ij})	=	controller matrix (element i, j)
$\boldsymbol{K}$, (k_{ij})	=	precompensator matrix (element i, j)
$\boldsymbol{L}$, (l_{ij})	=	loop transmission function matrix (element i, j)
$\boldsymbol{P}$, (p_{ij})	=	plant model matrix (element i, j)
q_{ij}	=	$1/p_{ij}$
R	=	yaw rate, deg/s
$\boldsymbol{R}$	=	input vector
T_s	=	sample time
$T_{Y/U}$, (t_{ij})	=	transfer function matrix (element i, j) from $\boldsymbol{U}$ to $\boldsymbol{Y}$
w	=	heave rate, ft/s
$\boldsymbol{Y}$	=	output vector
α_{ij}	=	design bound specification for prefilter element design
β	=	trim variable
γ	=	climb angle
γ, $(\gamma_{\max})$	=	interaction (maximum) index
δ_a, δ_c, δ_e, δ_r	=	lateral cyclic, main rotor collective, longitudinal cyclic, and tail rotor collective, respectively, deg
ζ	=	damping factor
τ	=	dummy variable of integration
τ, $(\tau_{\max})$	=	phase (maximum) delay
ϕ, (θ)	=	roll (pitch) angle, deg
$\phi_{2\omega 180}$	=	two times the frequency of the −180-deg phase
ω, ω_n, ω_{BW}, $\omega_{\mathrm{BW}_{\mathrm{phase}}}$, $\omega_{\mathrm{BW}_{\mathrm{gain}}}$, ω_{180}	=	frequency (rad/s), natural frequency, bandwidth frequency, phase bandwidth frequency, gain bandwidth frequency, and phase crossover frequency, respectively

Received 11 February 1999; revision received 15 July 1999; accepted for publication 10 January 2000.

*Graduate Student, Department of Mechanical Engineering.
†Late Professor and Chair, Department of Mechanical Engineering.
‡Professor, Department of Electrical Engineering.

Introduction

FUNDAMENTAL problems in helicopter control at hover (low-speed flight up to approximately 45 knots) include interactions between the longitudinal and lateral axes, coupling of the control inputs, inherent low-frequency instability, and insufficient bandwidth for level-1 flying qualities.[1] These lead to increased pilot workload. These factors, in addition to the high degree of uncertainty that exists both in the helicopter dynamics and the mathematical modeling assumptions that give rise to linearized models, necessitate a robust controller. The time-invariant linear models used embody the important aerodynamic, structural, and other internal dynamic effects that collectively influence the response of the helicopter to the pilot's controls and external disturbances. The controller must account for both unstructured uncertainties from modeling inaccuracy and the structured parametric uncertainty that arises because of the different flight conditions. The quantitative feedback theory (QFT) is well suited to controller design for systems with large parameter uncertainty for which it is required to meet, point-wise, closed-loop frequency domain performance tolerances.[2–6] In Refs. 7 and 8 the QFT method was used to design the controllers. The Perron root of the interaction matrix was used in Ref. 8 as a measure of the level of triangularization of the model and in the design objective for the compensator. In Ref. 7 a cross-feed was designed to achieve decoupling before QFT was applied to obtain diagonal controllers. The method used in finding the low-order cross-feeds from the Linear Control Analysis Program generates ideal cross-feeds and runs into difficulty when good approximations to the ideal cross-feed cannot be obtained because of scattering of the so-called target points at each frequency. This leads to undesirable roll angle and heave rate responses caused by a change in the longitudinal cyclic. This paper makes use of the Perron root of the interaction matrix as a measure of the level of interaction of the system.

We consider the two-degree-of-control-freedom, four-input, four-output helicopter. The model used here is the UH-60 Black Hawk helicopter, which is a four-blade, articulated rotor, utility helicopter. We examine the use of quantitative cross-feed design followed by diagonal feedback design to decouple, stabilize, and improve handling

qualities of the helicopter for near-hover operations. Because the control hardware will be digital, the design is undertaken directly in the discrete w domain, the bilinear Tustin transformation of the z domain $[z = (1 + wT/2)/(1 - wT/2),\ (2z - 1)/(Tz + 1)]$. The system inputs and outputs are defined in Table 1.

The models were obtained by linearization of an accurate nonlinear model about different operating points at hover and near-hover conditions using the program FORECAST.[9] The qualitative classification of the probability of occurrence is shown for 24 flight conditions (#11 not included) in Appendix A. Forward-loop precompensation (cross-feed) design seeks to reduce the interaction index before quantitative design of a diagonal feedback controller matrix is attempted. If the interaction index can be made to be less than unity by the design, stability of the diagonal-loop designs guarantees stability of the closed-loop multivariable system. The design presented here serves as an example of a dynamic precompensator design in contrast to the static precompensator presented in Ref. 8. Also, in this paper we introduce differentiated specifications. Some level of open-loop decoupling can be useful for improving practical pilot handling qualities even if the feedback loops are opened, for example, because of sensor failure or when the autopilot is not used.

The remainder of this paper is divided as follows: the next section discusses the helicopter model and the formulation of the design problem. A detailed design for the helicopter follows after a brief review of the Perron root theory and the underlying theory upon which the design is based. Simulation results for the design compared to ADS-33D-PRF are presented next followed by the conclusion.

Background-to-Design Model

The model treats the helicopter as a six degree-of-freedom rigid fuselage with rigid rotor blades each with a flap and lag degree of freedom. The model has 45 states with 6 states attributable to the body motion, 16 states defining the flap and lag motions of the rotor, 2 states describing the dynamic twist, 4 states representing the dynamic inflow, 6 states defining the engine dynamics, 8 states describing the primary servo dynamics, 2 states defining the downwash and sidewash of the tail rotor, and 1 state defining the blade azimuth error.[7] At most, 33 state variables are retained in the linear models for the hover conditions. This paper considers a nominal hover condition and 23 near-hover conditions. The nominal hover condition is for a rotor speed of 27 rad/s, gross weight of 16,825 lbs (7632 kg), and air density at a standard sea-level value of 0.002377 slug/ft^3 (1.2255 kg/m^3) (Ref. 7). Other near-hover conditions are obtained as the trim airspeed, rotor speed, and other parameters are varied. When there is no forward speed (hover situation), there is high control sensitivity because of low damping, and this makes the helicopter prone to pilot-induced oscillations (PIO), thereby increasing the difficulty of the pilot's task. Also the helicopter is susceptible to gusts, and all of these add to pilot load. The design problem includes the sampling effects, computational delay, actuator and sensor dynamics summarized in Table 2.

Table 1 Input-output pairings for helicopter control

Input	Output
δ_a = lateral cyclic, deg	ϕ = roll angle, deg
δ_e = longitudinal cyclic, deg	θ = pitch angle, deg
δ_c = main rotor collective pitch, deg	w = heave velocity, ft/s
δ_r = tail rotor collective, deg	R = yaw rate, deg/s

These effects are appended to the helicopter model to obtain the final plant model $\boldsymbol{P}$. The control system structure is shown in Fig. 1, which can be reduced to the classical two-degree-of-freedom structure in Fig. 2. The input vector $\boldsymbol{U}$ and output vector $\boldsymbol{Y}$ are ordered as shown in Table 1.

Problem Formulation

The ADS-33D-PRF defines the minimum response characteristics that will allow various mission task elements (MTEs) to be met at a particular level of handling quality.[10] As explained in Ref. 11, experience acquired through flight simulation and test data has shown a number of response characteristics relevant to achieving good handling qualities, which are specified as a function of the usable cue environment (UCE) and MTEs.[12] Based on these, an attitude-hold-attitude-command response type (ACAH), a requirement for satisfactory handling qualities in the hover/low-speed flight region, was chosen for this design. The QFT tracking problem is then stated as follows:

Given the system in Fig. 2, where $\boldsymbol{P} \in \wp$, the plant set, design $\boldsymbol{G}$, $\boldsymbol{K}$, and $\boldsymbol{F}$ such that

$$a_{ij}(\omega) \le |\boldsymbol{T}_{Y/R}(j\omega)|_{ij} \le b_{ij}(\omega), \qquad i, j = 1, 2, 3, 4 \tag{1}$$

where $a_{ij}(\omega)$ and $b_{ij}(\omega)$ are desired specifications to ensure required flying quality and $|\boldsymbol{T}_{Y/R}(j\omega)|_{ij}$ is the magnitude of the ijth element of the closed-loop command response function $\boldsymbol{T}_{Y/R}(s)$. We design the principal channels ($i = j$) to obtain the minimum loop sensitivity possible while maximizing the loop bandwidth. The prefilter is then used to enhance this first cut design to ensure that level-1 flying quality is obtained.

Pitch-Angle and Roll-Angle Requirements

The control and decoupling requirements for the pitch and roll axes are similar because of symmetry of the helicopter about the

Table 2 Time delay contributions to the control system

Effect	Model	Comment
Actuator dynamics	$1521/(s^2 + 54.6s + 1521)$	Before transformation to z domain
Computational delay 1 sample at 15 ms	$(1 - wT/2)/(1 + wT/2) = z^{-1}$	Exact
Sensor dynamics (antialiasing filter)	$6024/(s^2 + 109.2s + 6084)$	Before transformation to z domain
Sampler effect T = 15 ms	$\simeq (1 - wT/2)$	Approximation in w domain[14]

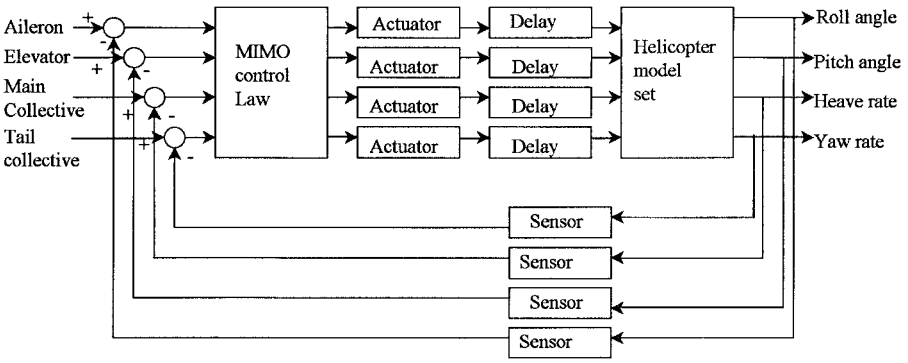

Fig. 1 Helicopter model with actuator, sensor, and delay models.

Table 3 Control design prefiltering

Axes	Upper limit	Lower limit
Roll	$3.9^2/(w^2 + 2 \times 0.35 \times 3.9w + 3.9^2)$	$1/(w/1 + 1)^3$
Pitch	$3.9^2/(w^2 + 2 \times 0.35 \times 3.9w + 3.9^2)$	$1/(w/1 + 1)^3$
Heave rate	$1/(w/3 + 1)$	$1/(w/2 + 1)$
Yaw rate	$1/(w/4 + 1)$	$1/(w/3 + 1)$

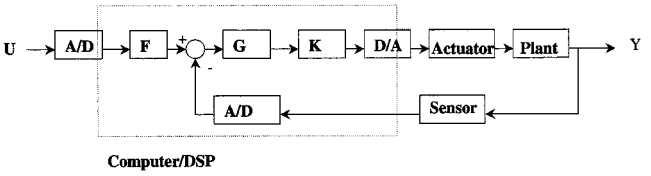

Fig. 2 Two-degree-of-freedom feedback structure.

lateral and longitudinal axes. The upper limit of the prefiltering transfer function for these axes is taken as a transfer function that will give a maximum overshoot of 3 dB (damping factor of 0.35) and a bandwidth of 5.5 rad/s. The lower limit is approximated by a transfer function that will ensure effective damping with natural frequency chosen to obtain a level-1 flying quality with a phase delay parameter (to be defined later) of 0.2 s. The decoupling requirements, which will be stated qualitatively in the evaluation section, require a certain maximum response in the roll angle (pitch angle) caused by the longitudinal cyclic (lateral cyclic).

Heave-Rate and Yaw-Rate Requirements

The heave-rate and yaw-rate axes prefiltering functions are obtained as first-order responses that achieve the limits for level-1 flying quality in the ADS-33D-PRF. The yaw rate requires a minimum bandwidth of 4 rad/s, whereas the heave rate requires a bandwidth of 2 rad/s. Noting that the s- and w-domain transfer functions are approximately the same for sufficiently fast sampling relative to the required bandwidth, the w-domain specifications for the principal axes are shown in Table 3. The heave-rate response caused by a change in the tail-rotor collective shall not be objectionable. The yaw-rate response caused by a unit step change in the main-rotor collective shall not exceed 5 deg/s.

MIMO Control Law Design

The frequency range of interest for piloted angle/rate commands (δ_a, δ_e, δ_r), obtained experimentally from the autospectrum of pilot inputs during the Advanced Digital Optical Control Systems study,[13] are 1.0–10.0 rad/s and for heave command (δ_c) from 0.2 to 2.0 rad/s. As the sampling rate has been fixed by previous studies, we get directly to the w-domain via[14]:

$$\begin{aligned}\boldsymbol{P}(w) &= \boldsymbol{P}_z(z)|_{z=(1+wT/2)/(1-wT/2)} \\ &= [\boldsymbol{C}_D(\boldsymbol{I}z - \boldsymbol{A}_D)\boldsymbol{B}_D]|_{z=(1+wT/2)/(1-wT/2)} \\ &\approx \boldsymbol{P}_s(w)(1 - wT/2) \end{aligned} \tag{2}$$

With

$$\boldsymbol{A}_D = e^{AT_s}, \quad \boldsymbol{B}_D = \int_0^{T_s} e^{A\tau}\,\mathrm{d}\tau \boldsymbol{B}, \qquad \boldsymbol{C}_D = \boldsymbol{C}, \qquad \left[\begin{array}{c|c} \boldsymbol{A} & \boldsymbol{B} \\ \hline \boldsymbol{C} & 0 \end{array}\right]$$

as the state-space system for the design model, which includes the plant, actuator, and sensor effects. Computational delay, $z^{-1} = (1 - wT/2)/(1 + wT/2)$, is added after discretization.

Basic Theory

The design will make use of the theory of nonnegative matrices, and the reader is referred to Refs. 15–17. Full details of the precompensator design are given in Ref. 18.

Definition 1: A matrix $\boldsymbol{M} \in R^{n\times n}$ is an M matrix if the diagonal elements of $\boldsymbol{M}$ are positive, the off diagonal elements of $\boldsymbol{M}$ are nonpositive, and the principal minors of $\boldsymbol{M}$ are nonnegative.

Definition 2: Given a matrix $\boldsymbol{Z} \in C^{n\times n}$, the comparison matrix of $\boldsymbol{Z}$, $M(\boldsymbol{Z})$ has elements

$$M(\boldsymbol{Z})_{ij} = \begin{cases} |z_{ii}| & \text{(diagonal elements)} \\ -|z_{ij}| & i \neq j \end{cases}$$

Definition 3: A matrix $\boldsymbol{Z} \in C^{n\times n}$ is irreducible if there does not exist a permutation $\boldsymbol{P} \in C^{n\times n}$ such that

$$\boldsymbol{PZP}^{-1} = \left[\begin{array}{c|c} \boldsymbol{Z}_{11} & \boldsymbol{Z}_{12} \\ \hline 0 & \boldsymbol{Z}_{22} \end{array}\right]$$

with square submatrices $\boldsymbol{Z}_{11}$ and $\boldsymbol{Z}_{22}$.

Definition 4: An irreducible matrix $\boldsymbol{Z} \in C^{n\times n}$ is an H matrix (Hadamard matrix) if $M(\boldsymbol{Z})$ is an M matrix.

Definition 5: An H matrix $\boldsymbol{Z} \in C^{n\times n}$ is a BH matrix if $\boldsymbol{Z}^{-1}$ is also an H matrix.

Definition 6: A matrix $\boldsymbol{Z}$ admits a diagonal regular splitting if it can be written as $\boldsymbol{Z} = \boldsymbol{D} + \boldsymbol{C}$, with $\boldsymbol{D} = \mathrm{diag}\{\boldsymbol{Z}\}$ nonsingular.

Definition 7: The Perron root of a matrix $\boldsymbol{M}$ is the largest eigenvalue of the matrix formed from the absolute values of the elements of $\boldsymbol{M}$.

$$\lambda_p(\boldsymbol{M}) = \max\{\lambda(\boldsymbol{M}_+)\} = \rho(\boldsymbol{M}_+)$$

where $\rho(\boldsymbol{M}_+)$ is the spectral radius of $\boldsymbol{M}_+$. The absolute values are taken element-wise, $(\boldsymbol{M}_+)_{ij} = |\boldsymbol{M}_{ij}|$. Corresponding to the Perron root are the right and left Perron eigenvectors $\boldsymbol{x}$ and $\boldsymbol{y}^T$, respectively. They can be scaled to give $\boldsymbol{y}^T\boldsymbol{x} = 1$, resulting in their elements being real and positive.

Definition 8: Given that $\boldsymbol{Z} \in C^{n\times n}$ admits the diagonal regular splitting,

$$\boldsymbol{Z} = \boldsymbol{D} + \boldsymbol{C} = (\boldsymbol{I} + \boldsymbol{C}\boldsymbol{D}^{-1})\boldsymbol{D} = (\boldsymbol{I} + \boldsymbol{M})\boldsymbol{D}$$

$\boldsymbol{M}$ is the interaction matrix, and the interaction index of $\boldsymbol{Z}$ is the Perron root of the interaction matrix $\gamma(\boldsymbol{Z}) = \lambda_P(\boldsymbol{M})$.

Let $\boldsymbol{Z}^{-1} = \hat{\boldsymbol{Z}}$. If $\boldsymbol{Z}$ is an H matrix, then $\rho(\boldsymbol{M}) \leq \lambda_p(\boldsymbol{M}) < 1$, and

$$(\boldsymbol{I} + \boldsymbol{M})^{-1} = \sum_{k=0}^{\infty} \boldsymbol{M}^k$$

converges. Also,

$$\gamma(\hat{\boldsymbol{Z}}) = \gamma[\boldsymbol{D}^{-1}(\boldsymbol{I} + \boldsymbol{M})^{-1}] = \lambda_P\left(\sum_{k=0}^{\infty} \boldsymbol{M}^k\right) \leq \sum_{k=0}^{\infty} [\lambda_P(\boldsymbol{M})]^k$$

$$= \frac{\gamma(\boldsymbol{Z})}{1 - \gamma(\boldsymbol{Z})} \tag{3}$$

If $\boldsymbol{Z}$ is row dominant,

$$|z_{ii}| > \sum_{k=1, k\neq i}^{n} |z_{ij}|$$

for all i, $\gamma(\boldsymbol{Z}) < 1$, so that dominance is a special case of requiring $\boldsymbol{Z}$ to be an H matrix. The same applies to column dominance.

Theorem 1: An irreducible matrix $\boldsymbol{Z} \in C^{n\times n}$ is a BH matrix if $\min\{\gamma(\boldsymbol{Z}), \gamma(\hat{\boldsymbol{Z}})\} \leq 0.5$

Definition 9: An irreducible matrix $\boldsymbol{Z} \in C^{n\times n}$ is almost decoupled if $\max\{\gamma(\boldsymbol{Z}), \gamma(\hat{\boldsymbol{Z}})\} \leq 0.5$.

Theorem 2: An H matrix $\boldsymbol{Z} \in C^{n\times n}$ is almost decoupled if $\gamma(\boldsymbol{Z}) \leq 1/3$.

Proofs for theorems 1 and 2: see Ref. 16, or follows from Eq. (3).

Theorem 3: Given a matrix $\boldsymbol{M}$ with a simple (nonrepeated) eigenvalue λ and the corresponding right and left eigenvectors $\boldsymbol{x}$ and $\boldsymbol{y}^T$,

scaled so that $\boldsymbol{y}^T\boldsymbol{x}=1$, the eigenvalue differential sensitivity with respect to element (i, j) of $\boldsymbol{M}$ is

$$\frac{\partial\lambda}{\partial m_{ij}} = y_i x_j \tag{4}$$

As λ and m_{ij} are positive, the logarithmic differential sensitivity (follows from Ref. 19) is

$$\frac{\partial\log(\lambda)}{\partial\log(m_{ij})} = \frac{m_{ij}}{\lambda} y_i x_j \tag{5}$$

Precompensator Design

The feedback structure gives the closed-loop transfer function as

$$\boldsymbol{T}_{Y/R} = (\boldsymbol{I}+\boldsymbol{PKG})^{-1}\boldsymbol{PKGF} \tag{6}$$

The sensor dynamics is taken as $\boldsymbol{H}=\boldsymbol{I}$ for simplicity because block diagram manipulation enables it to be put in the forward path. Writing Eq. (6) implicitly gives

$$(\hat{\boldsymbol{P}}+\boldsymbol{KG})\boldsymbol{T}_{Y/R} = \boldsymbol{KGF} \tag{7}$$

or

$$(\hat{\boldsymbol{K}}\hat{\boldsymbol{P}}+\boldsymbol{G})\boldsymbol{T}_{Y/R} = \boldsymbol{GF} \tag{8}$$

In Eq. (7), $\hat{\boldsymbol{P}}=\boldsymbol{P}^{-1}$ with elements $\hat{p}_{ij}=1/q_{ij}$. This can also be written as

$$\boldsymbol{T}_{Y/R}\hat{\boldsymbol{F}}(\boldsymbol{PK}+\hat{\boldsymbol{G}}) = \boldsymbol{PK} \tag{9}$$

Rosenbrock[20] showed that any controller can be decomposed as a product of a permutation matrix, a unimodular matrix, and a diagonal matrix. The diagonal matrix will be $\boldsymbol{G}$, and the unimodular matrix will be the $\boldsymbol{K}$ or $\hat{\boldsymbol{K}}$ in Eqs. (8) or (9), respectively. Considering Eq. (8), we can write

$$\hat{\boldsymbol{K}} = \hat{\boldsymbol{K}}_r\cdots\hat{\boldsymbol{K}}_2\hat{\boldsymbol{K}}_1 \tag{10}$$

For each step h of the design (and corresponding i and j), $\hat{\boldsymbol{K}}_h = \boldsymbol{I}+\hat{k}_{ij}\boldsymbol{E}_{ij}$ with $\boldsymbol{E}_{ij}$ an elementary matrix having element (i, j) unity and all other elements zero. Define

$$\hat{\boldsymbol{P}}^h = \prod_{k=1}^{h}\hat{\boldsymbol{K}}_k\hat{\boldsymbol{P}}^k = \hat{\boldsymbol{K}}_h\hat{\boldsymbol{P}}^h \tag{11}$$

$\hat{\boldsymbol{K}}_h$ only affects the ith row of $\hat{\boldsymbol{P}}^h$

$$\hat{p}_{ik}^{h+1} = \hat{p}_{ik}^h + k_{ij}\hat{p}_{jk}^h$$

Equation (6) is written implicitly as

$$(\hat{\boldsymbol{P}}^{h+1}+\boldsymbol{G})\boldsymbol{T}_{Y/R} = \boldsymbol{G} = (\hat{\boldsymbol{K}}^h\hat{\boldsymbol{P}}^h+\boldsymbol{G})\boldsymbol{T}_{Y/R} \tag{12}$$

and with diagonal splitting

$$(\hat{\boldsymbol{P}}^{h+1}+\boldsymbol{G}) = \left(\hat{\boldsymbol{P}}_D^{h+1}+\boldsymbol{G}\right)(\boldsymbol{I}+\boldsymbol{M}^{h+1})$$

with interaction matrix

$$\boldsymbol{M}^{h+1} = \left(\hat{\boldsymbol{P}}_D^{h+1}+\boldsymbol{G}\right)^{-1}\hat{\boldsymbol{P}}_0^{h+1}$$

of individual elements

$$m_{ik}^{h+1} = \frac{\hat{p}_{ik}^{h+1}}{\hat{p}_{ii}^{h+1}+g_i} = \frac{\hat{p}_{ik}^h + \hat{k}_{ij}\hat{p}_{jki}^h}{\hat{p}_{ii}^1+\hat{k}_{ij}\hat{p}_{ji}^h g_i}$$

In step h the interaction index is only changed as a result of changes in row i. We can therefore approximate the change in the interaction index, and using some design insights,[18] justify only examining the jth element, giving

$$\underset{\text{element } ij}{\Delta}\log[\lambda^{(h+1)}] \approx \Delta\log(m_{ij})\frac{\partial\log(\lambda)}{\partial\log(m_{ij})}$$

$$\approx \log\left[\frac{\left(\hat{p}_{ij}^h+k_{ij}\hat{p}_{jj}^h\right)}{\left(\hat{p}_{ii}^h+k_{ij}\hat{p}_{ji}^h+g_i\right)}\frac{\left(\hat{p}_{ii}^h+g_i\right)}{\left(\hat{p}_{ij}^h\right)}\right]^{|m_{ij}|y_i x_j/\lambda^{(h)}} \tag{13}$$

with $\mathcal{L}_i = g_i/\hat{p}_{ii}$ and

$$\beta_{ij}^h = \left[\frac{\lambda_d^{(h+1)}}{\lambda^{(h)}}\right]^{\lambda^{(h)}/|m_{ij}^{h1}|(y_i x_j)^h}$$

an appropriate design task is to achieve

$$\left|\frac{\hat{p}_{ij}^h+k_{ij}\hat{p}_{jj}^h}{\hat{p}_{ii}^h+k_{ij}\hat{p}_{ji}^h}\right| \le \beta_{ij}^h\left|\frac{\hat{p}_{ij}^h}{\hat{p}_{ii}^h}\right|\left|\frac{1+\mathcal{L}_i^{h+1}}{1+\mathcal{L}_i^h}\right|$$

Because the diagonal sensitivity depends on the specifications and changes in gain between $\hat{p}_{ii}^h$ and $\hat{p}_{ii}^{h+1}$ and will be approximately compensated by changes in g_i,

$$\left|\frac{1+\mathcal{L}_i^{h+1}}{1+\mathcal{L}_i^h}\right| \approx 1$$

and the design objective is

$$\left|\frac{1+k_{ij}\hat{p}_{jj}^h/\hat{p}_{ij}^h}{1+k_{ij}\hat{p}_{ji}^h/\hat{p}_{ii}^h}\right| \le \beta_{ij}^h \tag{14}$$

The design of the cross-feed (4, 3) element, from measured heave-rate controller output to tail-rotor collective input, is done to illustrate the design procedure of obtaining the precompensators. The minimum product of interaction index sensitivity and M matrix element $|m_{ij}|(y_i x_j)$ for the off-diagonal elements of $\hat{\boldsymbol{P}}$ are most significant for elements (1, 4) and (4, 3). Investigation showed the other elements did not cause any significant reduction in the interaction index.

Different constraints are applied to two model subsets by specifying improved performance in the more probable cases ({More Probable} = {Most Probable} ∪ {Less Probable}) at the expense of lower but still acceptable performance in the least-probable cases. The (4, 3) cross-feed design has the following structure:

$$\hat{\boldsymbol{K}}_h\hat{\boldsymbol{P}}^h = \hat{\boldsymbol{P}}^{(h+1)}$$

$$\begin{pmatrix}1&0&0&0\\0&1&0&0\\0&0&1&0\\0&0&\hat{k}_{43}&1\end{pmatrix}\begin{pmatrix}\hat{p}_{11}&\hat{p}_{12}&\hat{p}_{13}&\hat{p}_{14}\\\hat{p}_{21}&\hat{p}_{22}&\hat{p}_{23}&\hat{p}_{24}\\\hat{p}_{31}&\hat{p}_{32}&\hat{p}_{33}&\hat{p}_{34}\\\hat{p}_{41}&\hat{p}_{42}&\hat{p}_{43}&\hat{p}_{44}\end{pmatrix}$$

$$=\begin{pmatrix}\hat{p}_{11}&\hat{p}_{12}&\hat{p}_{13}&\hat{p}_{14}\\\hat{p}_{21}&\hat{p}_{22}&\hat{p}_{23}&\hat{p}_{24}\\\hat{p}_{31}&\hat{p}_{32}&\hat{p}_{33}&\hat{p}_{34}\\\hat{p}_{41}+\hat{k}_{43}\hat{p}_{31}&\hat{p}_{42}+\hat{k}_{43}\hat{p}_{32}&\hat{p}_{43}+\hat{k}_{43}\hat{p}_{33}&\hat{p}_{44}+\hat{k}_{43}\hat{p}_{34}\end{pmatrix}$$

Figure 3 illustrates the interaction index for the uncompensated plant $\boldsymbol{P}$. It is expected that either through the action of the pilot or diagonal controller (autopilot) acceptable performance can be obtained at frequencies below 1 rad/s. Decoupling by means of cross-feed is therefore required in the gain crossover region, from 1 to 10 rad/s. Figure 4 shows the detail of the worst (maximum) cases for {Most Probable}, {Less Probable}, and {Least Probable} subsets in this design region. Figure 4 also shows the following client specifications for interaction reduction:

1) {More Probable}: $\lambda_{\text{spec}} \le \min\{0.9, 0.8\times\lambda\}$.

2) {Least Probable}: $\lambda_{\text{spec}} \le \min\{1.2, 0.8\times\lambda\}$, $\lambda_{\text{spec}} \le 1.4$ for $\omega \le 1.25$.

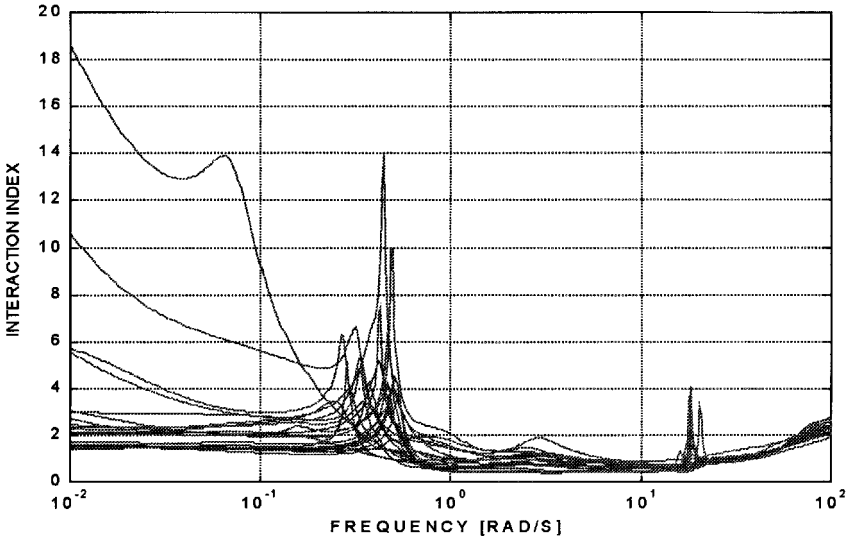

Fig. 3 Interaction index of plant set before precompensation.

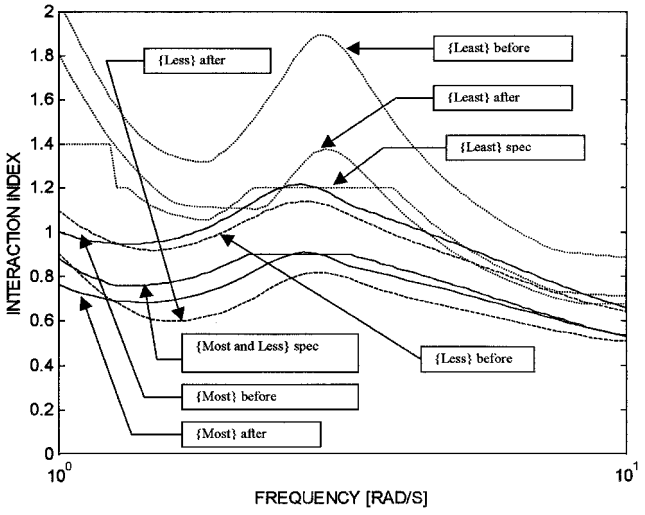

Fig. 4 Detail of worst cases of open-loop interaction index and specifications in Refs. 1 and 10 radians/second and reduction in interaction index by $k43$ and $k14$ design.

Knowledge about what is achievable and the extent of tradeoff permissible between the plant subsets is embedded in these specifications. Using these values, the design in Eq. (14) becomes,

$$\left|\frac{1+\hat{k}_{43}\hat{p}_{33}/\hat{p}_{43}}{1+\hat{k}_{43}\hat{p}_{34}/\hat{p}_{44}}\right| \le \beta_{43} \qquad \text{with} \qquad \beta_{43} = \left(\frac{\lambda_{\text{spec}}}{\lambda}\right)^{\lambda/|m_{43}|(y_4x_3)} \tag{15}$$

The log-polar plane (modified Nichols Chart) in Fig. 5 shows the design bounds on $\hat{k}_{43}$ at $\omega = 2$ for the entire plant set. If a single specification had been used for all of the elements of the plant set, each would have generated a small feasible region, and the intersection of these feasible regions would have no intersection. As shown in Fig. 5, the specifications have been made so tight that the intersection is very small. Figure 6 (with different scale) shows the intersection of bounds (as a shaded region) for the {More Probable} and {Least Probable} subset specifications independently at the design frequencies, $\omega = [1, 1.5, 2, 3, 4, 6, 8, 10]$ rad/s. It also shows the cross-feed design given by the stable but nonminimum phase lag

$$k_{43} = \frac{-0.125(s/2.1+1)(s/(-1.6)+1)}{(s/2.4)^2 + 2\times 0.4 \times s/2.4 + 1} \tag{16}$$

This design satisfies the {Most Probable} specifications, but as the intersection of the specification bounds is empty at most frequencies, it cannot satisfy simultaneously the {Most Probable} and {Least Probable} specifications. Also shown in Fig. 4 is the reduction in worst-case interaction index for the three cases. As explained from Fig. 6, the specifications for the {Least Probable} set have not been met, and there are less serious violations of the specifications for the {More Probable} cases because β_{43} was based on differential sensitivity considerations. The cross-feed (1, 4) element, from measured yaw-rate controller output to lateral cyclic input, is obtained in a similar fashion but is not shown here because of space constraints. It is

$$k_{14} = \frac{0.042((w/0.8)^2 + 2\times 0.6 \times w/0.8 + 1)}{[(w/2)^2 + 2\times 0.7 \times w/2 + 1](w/30+1)}$$

A small interaction index reduces the need for high gains when the diagonal controllers are designed. A high bandwidth may excite fast modes or result in actuator rate and amplitude limiting.[21] The design of the diagonal controller will be carried out next.

Diagonal Controller Design

The transfer function from the reference to the output is given from Fig. 2 as

$$\boldsymbol{T}_{Y/R} = (\boldsymbol{I} + \boldsymbol{PKG})^{-1}\boldsymbol{PKGF} = (\hat{\boldsymbol{P}}^* + \boldsymbol{G})^{-1}\boldsymbol{GF} \tag{17}$$

where

$$(\hat{\boldsymbol{P}}^*)_{ij} = (\boldsymbol{PK})^{-1}_{ij} = 1/q^*_{ij}, \qquad l_i = g_{ii}q^*_{ii}$$

The requirement to guarantee the decoupled stability result of Ref. 8 is to ensure $\gamma|1/(1+l_i)| \le 1$ for the four loops over the entire frequency range $\omega \in (0.1, 10)$. Investigation showed it is impossible to satisfy this requirement for the four loops. Hence, tradeoffs will be made in the sequential loop design with the strategy being to minimize loop sensitivity while maximizing the loop bandwidth. In addition, the robust stability condition $|1/(1+l_i)| \le 3$ dB will be imposed for each loop.

Design of g_1

Generally, loops 1 and 2 for the pitch and roll angles have the highest bandwidth. As a result, the design for loop 1 will be carried out first. Modest design specifications are used in the first loop to minimize loop sensitivity with the hope of making improvements in subsequent loop designs. Our experience with QFT design is that the approach of overbounding design equations with the specifications, thereby neglecting phase information and the effects of ordering among plant cases, often leads to designs requiring unrealistic or

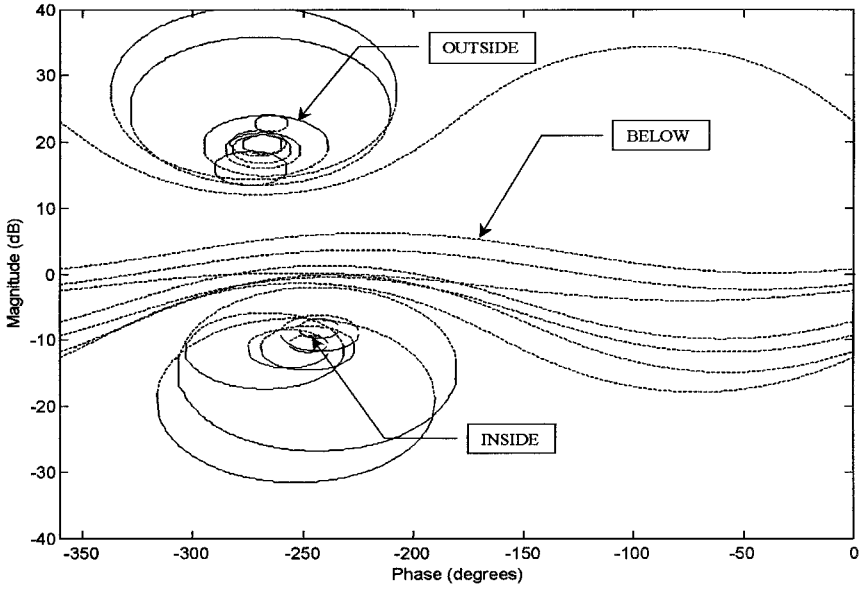

Fig. 5 Design bounds on $k43$ at $w = 2$.

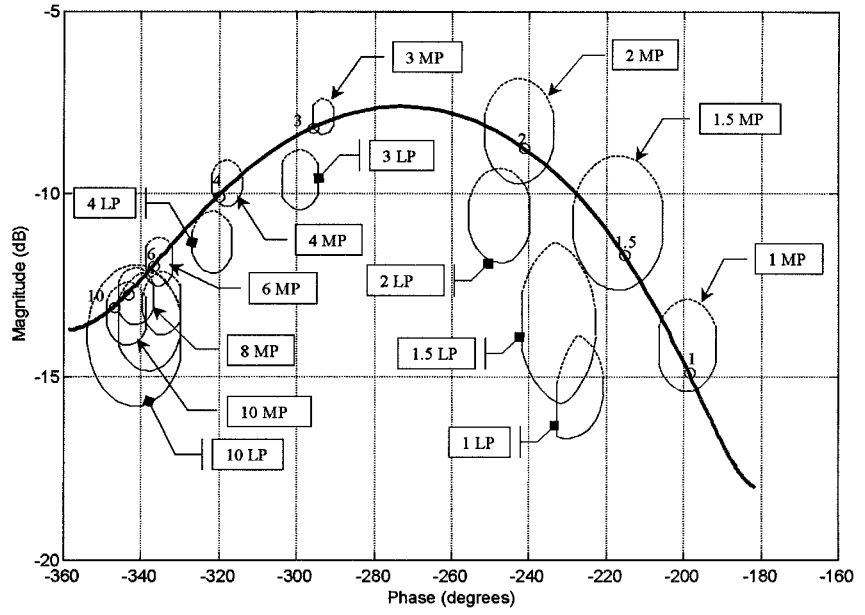

Fig. 6 Interaction of bounds and design of $k43$.

unachievable bandwidth to meet the user's requirements. The decoupled stability result of Ref. 8 cannot be satisfied across the whole frequency range so specifications are set as follows:

1) $|1/(1 + l_1)| \leq 3$ dB @ $\omega \leq 6$ rad/s.
2) $|1/(1 + l_1)| \leq 0$ dB @ $\omega = 0.1$–1 rad/s.

The bounds are obtained using the QFT toolbox[22] in MATLAB® and loop shaping gives the controller g_1 as

$$g_1 = \frac{20[(w/0.25) + 1][(w/4.9)^2 + 2^*0.5(w/4.9) + 1]}{[(w/0.1) + 1][(w/8) + 1][(w/30)^2 + 2^*0.5(w/30) + 1]}$$

Design of g_2

As in the design of g_1, the design specifications must be modest. Again, with the objective of minimizing sensitivity, we will design to achieve the following:

1) $|1/(1 + l_1)| \leq 3$ dB @ $\omega \leq 6$ rad/s.
2) $|1/(1 + l_1)| \leq 0$ dB @ $\omega = 0.1$–1 rad/s.

These bounds are generated via MATLAB® with the controller obtained as

$$g_2 = \frac{12[(w/2) + 1](w/6.5 + 1)}{(w/30 + 1)[(w/20)^2 + w/20 + 1]}$$

Design of g_3

Following the method of the last section, the design of loop three is carried out next to achieve the maximum loop bandwidth with bounds:

1) $|1/(1 + l_3)| \leq 0$ dB @ $\omega \leq 4$–18 rad/s.
2) $|1/(1 + l_3)| \leq 3$ dB @ $\omega = 3.5$ rad/s.

Loopshaping in MATLAB® gives the controller for the third loop as

$$g_3 = \frac{-0.9[(w/1.3) + 1][(w/6.5)^2 + 2^*0.8(w/6.5) + 1]}{w[(w/18) + 1][(w/16) + 1][(w/2.9) + 1]}$$

Design of g_4

With the design of the controllers for the first three loops complete, more realistic bounds are set for loop 4:

1) $|1/(1 + l_4)| \leq 0$ dB @ $\omega \leq 0.1$–3 rad/s.
2) $|1/(1 + l_4)| \leq 3$ dB @ $\omega = 6$ rad/s.
3) $|l_4/(1 + l_4)| \leq 2$ dB @ $\omega = 5.5$ rad/s.

Figure 7 shows a screen capture of the loop-shaping environment for loop 4. To satisfy the bounds, the curve at the various frequencies

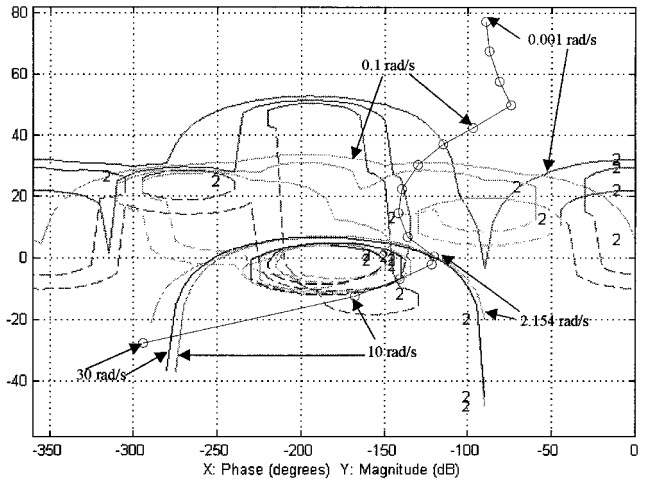

Fig. 7 Loop shaping for loop 4 (yaw rate).

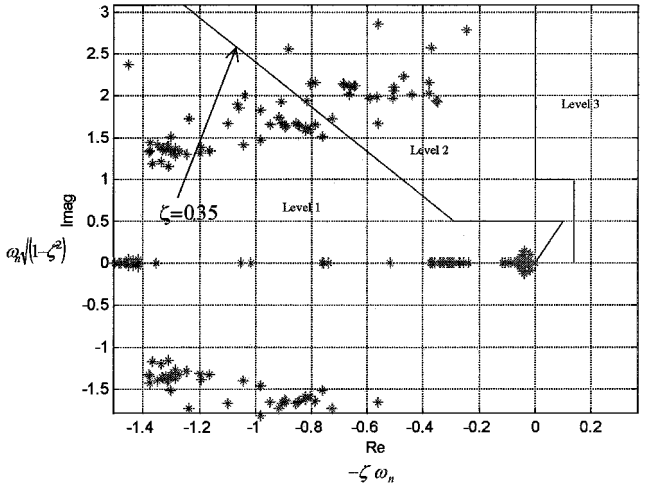

Fig. 8 Closed-loop poles showing boundaries for different handling qualities.

must be above or on the solid bounds and below or on the broken bounds at the respective frequencies. The controller for loop 4 is given as

$$g_4 = \frac{7.5[(w/1.5) + 1]}{w[(w/20) + 1]}$$

Closed-Loop Stability

Analysis of the system shows that the diagonal controllers achieve stability. The closed-loop poles are shown in Fig. 8. Stability of the closed-loop system was achieved despite the interaction index γ not being less than unity for all frequencies over the whole plant set. This would have simplified the single-input/single-output (SISO) design as well as guaranteed stability of the closed-loop MIMO system given stability of the SISO loops.

Design of Off-Diagonal Prefilters

$$\boldsymbol{T}_{Y/R} = (\boldsymbol{I} + \boldsymbol{PKG})^{-1}\boldsymbol{PKGF} = (\boldsymbol{I} + \boldsymbol{L})^{-1}\boldsymbol{LF} \tag{18}$$

where $\boldsymbol{L} = \boldsymbol{PKG}$ is the loop transmission function matrix. The design of off-diagonal prefilter elements can further reduce the interaction in the responses. The effect of the off-diagonal response can be reduced with respect to the on-diagonal response by finding the effect of f_{ij} on $(\boldsymbol{I} + \boldsymbol{L})^{-1}\boldsymbol{L}$, that is, $(\boldsymbol{I} + \boldsymbol{L})^{-1}\boldsymbol{L}\,[\boldsymbol{f}_{ij}]$ where $|\boldsymbol{f}_{ij}|$ is a matrix with unit diagonal elements, element f_{ij} to be designed, and all other elements as zero. The off-diagonal elements of

Table 4 Off-diagonal prefilters

Channel	Prefilter
f_{12}	$\dfrac{0.01[(w/0.2) + 1][(w/1.5 + 1]}{[(w/1.5)^2 + 2{*}0.5(w/15) + 1][(w/15) + 1]}$
f_{13}	$\dfrac{-0.01[(w/0.77) + 1]^2}{[(w/3.8)^2 + 2{*}0.65(w/3.8) + 1][(w/4.5)^2 + 2{*}0.7(w/4.5) + 1]}$
f_{14}	$\dfrac{-0.1[(w/1.5) + 1]}{[(w/3.5)^2 + 2{*}0.5(w/3.5) + 1]}$
f_{23}	$\dfrac{-0.008[w/(-12) + 1]}{\{[(w/7.5)]^2 + 2{*}0.5(w/7.5) + 1\}}$
f_{24}	$\dfrac{0.04[(w/0.1) + 1][(w/1.1) + 1][w/(-40) + 1]}{[(w/0.5)^2 + 2{*}0.9(w/0.5) + 1][(w/4.5)^2 + 2{*}0.5(w/4.5) + 1]}$
f_{34}	$\dfrac{-0.007(w/0.7 + 1)(w/30 + 1)}{[(w/10)^2 + 2{*}0.8(w/10) + 1]}$

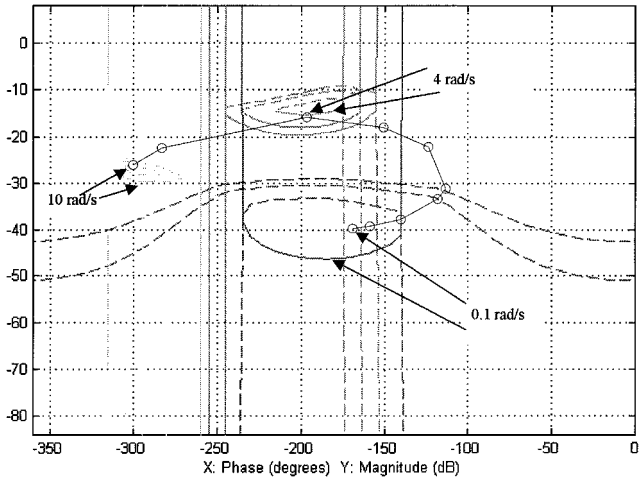

Fig. 9 Design of prefilter element (1, 3).

$(\boldsymbol{I} + \boldsymbol{L})^{-1}\boldsymbol{L}\,[\boldsymbol{f}_{ij}]$ must be as small as possible with respect to the on-diagonal elements. This reduces to finding bounds of the form

$$\left|\frac{t_{ii}f_{ij} + t_{ij}}{t_{ji}f_{ij} + t_{jj}}\right| \le \alpha_{ij} \tag{19}$$

where t_{ij} is the (i, j) element of the transfer function $(\boldsymbol{I} + \boldsymbol{L})^{-1}\boldsymbol{L}$, f_{ij} is the prefilter element being designed, and α_{ij} is a design bound specification. The idea is to make α_{ij} as small as possible over the frequency range. Design bound specifications of $0.9t_{ij}$, $0.75t_{ij}$, and $0.5t_{ij}$ were chosen over the whole frequency range, and their intersection was used to design the prefilter elements on the inverse Nichols chart using the QFT toolbox. Only the prefilters for the upper triangular elements were used. The lower triangular elements did not yield any further reduction in the off-diagonal response. The design of prefilter element f_{13} is shown in Fig. 9. The prefilters obtained are shown in Table 4.

Design of Diagonal Prefilter Elements

The transfer function for the two-degree-of-freedom structure in Fig. 2 is given by

$$\boldsymbol{T}_{Y/R} = (\boldsymbol{I} + \boldsymbol{PKG})^{-1}\boldsymbol{PKGF} = (\boldsymbol{I} + \boldsymbol{L})^{-1}\boldsymbol{LF} = \boldsymbol{T}_{\mathrm{BF}}\boldsymbol{F} \tag{20}$$

where $\boldsymbol{T}_{\mathrm{BF}}$ is the closed-loop transfer function before the diagonal prefilter elements are added. Prefilters for the principal axes are obtained in a straightforward manner in the form

$$|a_{ij}(j\omega)| \le |1_i f_{ii}/(1 + l_i)| \le |b_{ij}(j\omega)| \tag{21}$$

with $a_{ij}(j\omega)$ and $b_{ij}(j\omega)$ given in Table 3. The diagonal prefilters are shown in Table 5.

Table 5 Diagonal prefilters

Channel	Transfer function
f_{11}	$\dfrac{2.4^*[(w/0.13)+1]}{[(w/0.05)+1][(w/10)+1][(w/2.58)+1]}$
f_{22}	$\dfrac{1}{[(w/1.8)+1][(w/3.9)^2+2^*0.35w/3.9+1]}$
f_{33}	$\dfrac{1}{[(w/3)+1][(w/1.41)+1]}$
f_{44}	$\dfrac{[(w/1.46)^2+2^*0.36w/1.46+1]}{[(w/1.46)^2+2^*0.5w/1.46+1][(w/7.6)+1]}$

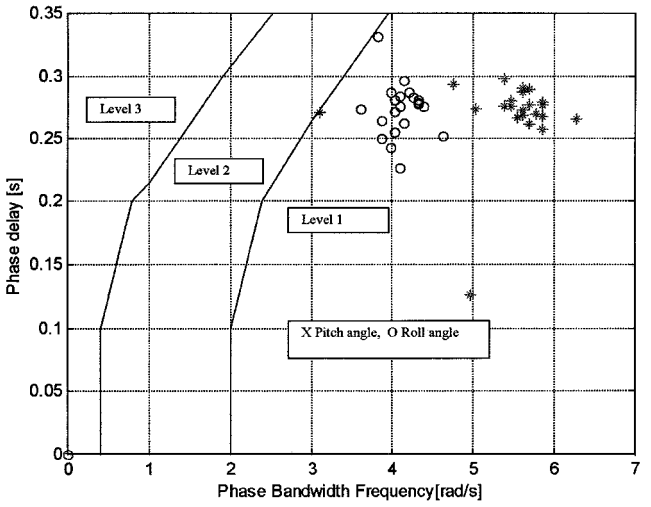

Fig. 10 Requirements for small-amplitude roll and pitch attitude changes (UCE > 1 and/or divided attention operations).

Evaluation for Handling Qualities

The ADS-33D-PRF is the basis for evaluation of the handling qualities. In this paper only the relevant performance specifications that can be evaluated by simulation are used. A full discussion of the handling qualities for rotorcraft is found in Refs. 12 and 23.

The closed-loop tracking tasks are characterized by the transmission bandwidth frequency ω_{BW}, which gives the system's ability to follow a range of input frequencies. There are two definitions of bandwidth frequency: gain margin ω_{BW}, $\omega_{BW_{gain}}$ and phase margin ω_{BW}, $\omega_{BW_{phase}}$ and are defined for second-order systems. $\omega_{BW_{gain}}$ is the frequency for 6 dB of gain margin, whereas $\omega_{BW_{phase}}$ is the frequency at which the phase margin is 45 deg. For the pitch and roll angles that have dominantly second-order responses ω_{BW}, damping ratio ζ, and natural frequency ω_n are related by

$$\omega_{BW} = \omega_n\left(\zeta + \sqrt{\zeta^2 + 1}\right) \tag{22}$$

Another important property used in helicopter dynamic response is the phase delay parameter τ_P.

It is a measure of how steep the phase drops off after -180 deg and is an indication of the behavior of the helicopter as the crossover frequency is increased. A large τ_P means a small margin between tracking at 45 deg of phase margin and instability, and increases susceptibility of the helicopter to PIO. A phase delay of 0.2 s or less is needed to have level-1 handling quality. τ_P is given[24] by

$$\tau_P = \frac{\Delta\Phi_{2\omega 180}}{57.3(2\omega_{180})} \tag{23}$$

where $\Phi_{2\omega 180}$ is the phase at twice the frequency of the -180-deg phase ω_{180}. For the ACAH-response type only the phase bandwidth is relevant. Simulation results are summarized here listing ADS-33D-PRF specifications and comments, with section numbers in parenthesis. (The section and page numbers refer to the ADS-33D-PRF.) A few of the least likely cases for the pitch angle do not quite fall within $\pm 10\%$ of the peak excursion. This requirement is satisfied for the most and less probable cases; character of attitude command response type (3.2.7, pp. 15)—a step cockpit pitch (roll) controller force input shall produce a proportional pitch (roll) attitude change within 6 s. The attitude shall remain essentially constant between 6 and 12 s following the step input. For aggressive maneuvering the roll (pitch) command inputs are 60 deg (30 deg). This requirement is satisfied with a low-frequency drift that can be reduced by the pilot; small-amplitude pitch (roll) attitude changes (3.3.2, pp. 17), short-term response to control inputs (bandwidth)—the limits (shown with the diagram) for the various levels of flying quality in the pitch (roll) responses to longitudinal (lateral) cockpit position inputs shall be satisfied. The boundaries are shown in Fig. 10 for the roll and pitch

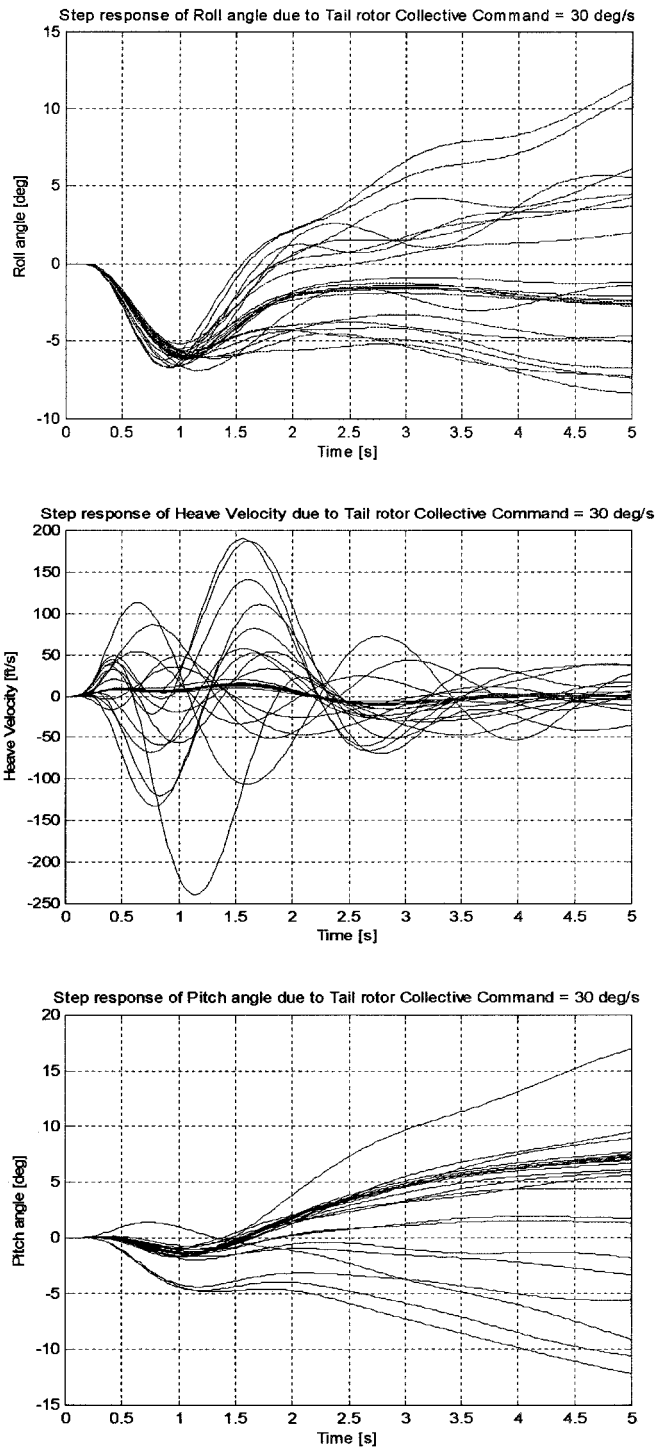

Fig. 11 Roll angle, heave rate and pitch angle responses due to a yaw rate input (tail rotor collective).

angles, and level 1 is achieved for all of the plants; small-amplitude pitch (roll) attitude changes (3.3.2.2, pp. 17), midterm response to control inputs—any oscillatory modes following a pulse controller input shall have an effective damping ratio of at least 0.35. For fully attended and divided operations the limits shown shall be met. For divided attention operations the damping shall not be less than $\zeta = 0.35$ at any frequency for level 1. This condition is satisfied by most of the poles, whereas a few satisfy level 2. See Fig. 8. Despite the oscillatory response seen in some of the results later in this section, the requirments of ADS-33D-PRF are satisfied as shown in Fig. 8; large-amplitude heading changes (3.3.8)—the achievable yaw rate in hover shall be no less than the specified values. The specified angular rates must be achieved about the yaw axis while limiting excursions in the other axes with the appropriate control inputs. The yaw rate satisfies the aggressive maneuvering MTEs. The responses of the roll angle, pitch angle, and heave velocity caused by a yaw-rate input (tail-rotor collective) are shown in Fig. 11; interaxis coupling (3.3.9.1), yaw caused by collective—the yaw-rate response to abrupt collective input with the directional controller free shall not exceed specified boundaries. Oscillations of yaw rates following step or ramp collective changes in the positive and negative directions shall not be greater than 5 deg/s. The maximum oscillation of yaw rate to collective command is about 0.012 deg/s per 1 ft/s, and level 1 flying quality is achieved. This is shown in Fig. 12; pitch-to-roll and roll-to-pitch coupling during aggressive maneuvering (3.3.9.2)—the ratio of peak off-axis attitude response from trim within 4 s to the desired (on-axis) attitude response from trim at 4 s following an abrupt lateral (longitudinal) control step input shall not exceed ± 0.25 for level 1 and ± 0.60 for level 2. Level 1 is achieved for most of the plants. For the pitch-to-roll average coupling is 0.26 with a standard deviation of 0.04. For the roll-to-pitch it is achieved with the maximum coupling of 0.18, average of 0.09, with a standard deviation of 0.04. The pitch-to-roll and roll-to-pitch responses are shown in Fig. 13. At very low frequencies acceptable performance can be obtained through the action of the pilot.

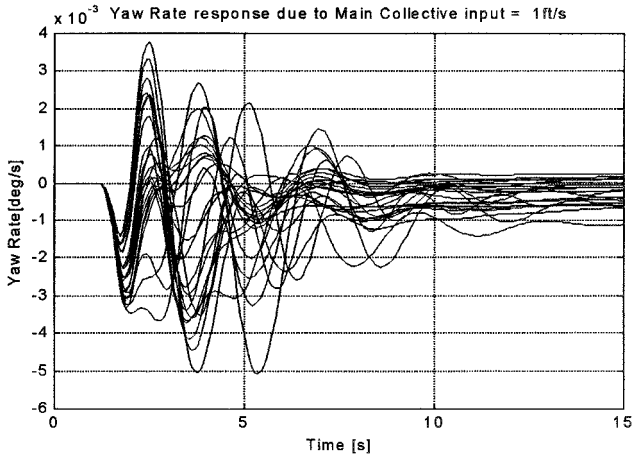

Fig. 12 Yaw-rate response caused by main-rotor collective.

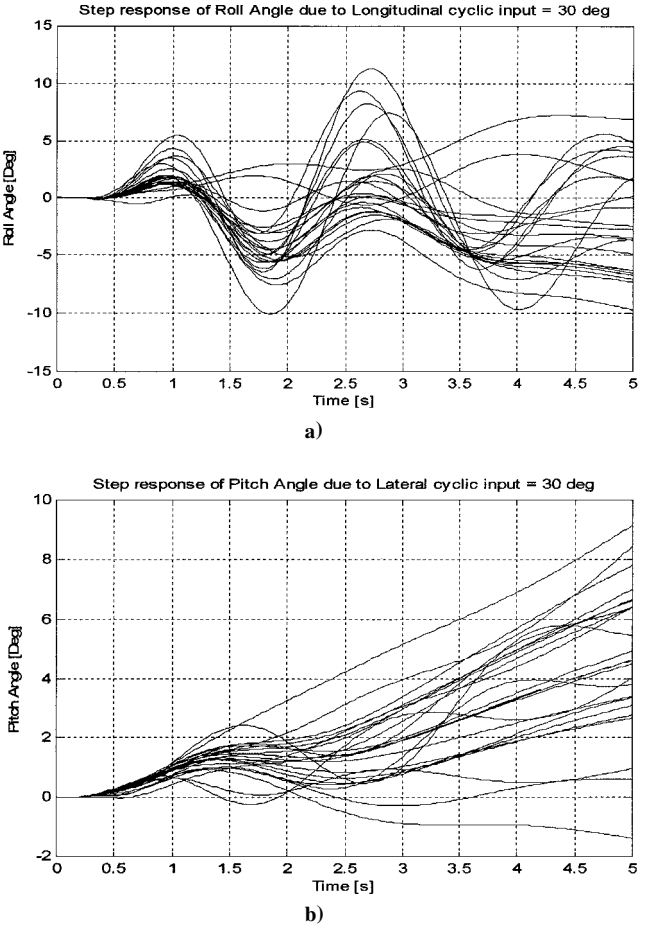

Fig. 13 Roll-to-pitch pitch-to-roll responses.

Conclusion

This paper has used the Perron root of the interaction matrix as a measure of the level of coupling in the linear model of the UH 60 Black Hawk helicopter. A dynamic decoupling precompensator has been used in the forward path to reduce the interaction that exists between the input and output variables. This eases the feedback loop design by reducing the controller bandwidth. By using the QFT, controllers have been designed for the individual loops to achieve stability and good flying qualities based on the ADS-33D-PRF. Most of the requirements for the helicopter at hover and near-hover flight conditions have been satisfied at level 1. For the least usual conditions level 1 was achieved in most of the cases, and level 2 was obtained where it was not possible to achieve level 1.

Appendix A: Table of Flight Configurations/Conditions

Table A1 Flight configurations/conditions

Probability	Flight configuration	Description
Most	1	Hovering
Most	2	15 kn* forward
Most	3	15 kn rearward
Most	7	15 kn, $\beta = 80$ deg
Most	9	15 kn, $\beta = -80$ deg
Less	6	15 kn, $\beta = 45$ deg
Less	8	15 kn, $\beta = -45$ deg
Less	14	6 kn, $\gamma = 80$ deg
Less	15	6 kn, $\gamma = -70$ deg
Least	4	30 kn forward
Least	5	30 kn, $\beta = -45$ deg
Least	10	30 kn, $\beta = 45$ deg
Least	12	30 kn, $\beta = -45$ deg
Least	13	30 kn, $\beta = -80$ deg
Least	16	12 kn, $\gamma = 80$ deg
Least	17	45 kn, $\gamma = -7.06$ deg, $\phi = 20$ deg (not trimmed)
Least	18	45 kn, $\gamma = -7.06$ deg $\phi = -20$ deg
Least	19	45 kn, $\gamma = 7.06$ deg, $\phi = 20$ deg
Least	20	Hovering, main rotor speed = 24 rad/s
Least	21	Hovering, main rotor speed = 30 rad/s
Least	22	Hovering, weight = 20,000 lbs
Least	23	45 kn, $\gamma = -7.06$ deg, $\phi = 20$ deg, weight = 20,000 lbs
Least	24	Hovering, forward c.g.
——	25	Hovering, aft c.g.

*1 kn = 0.5148 m/s.

Appendix B: Table of States Used in the FORECAST Model

Table B1

State index	Name	Description
1	u	forward velocity
2	v	sideward velocity
3	w	heave
4	p	roll rate
5	q	pitch rate
6	r	yaw rate
7	phi	roll angle
8	theta	pitch angle
9	psi	yaw angle
10	beta_0-dot	collective flap rate
11	beta_1c-dot	longitudinal flap rate
12	beta_1s-dot	lateral flap rate
−1[a]	beta_2-dot	differential flap rate
13	beta_0	collective flap
14	beta_1c	longitudinal flap
15	beta_1s	lateral flap
−1	beta_2	differential flap
16	zeta_0-dot	collective lag rate
17	zeta_1c-dot	longitudinal lag rate
18	zeta_1s-dot	lateral lag rate
−1	zeta_2-dot	differential lag rate
19	zeta_0	collective lag
20	zeta_1c	longitudinal lag
21	zeta_1s	lateral lag
−1	zeta_2	differential lag
22	phi_dyn	dynamic twist
23	phi_dyn-dot	dynamic twist rate
24	lambda	constant inflow
25	lambda_1c	first harmonic cos inflow
26	lambda_1s	first harmonic sin inflow
27	lambda_t	tail rotor inflow
28	nu_x	delayed downwash on tail
29	nu_y	delayed sidewash on tail
30	psi	blade azimuth error
31	omega	rotor speed
32	n_g	gas generator speed
33	w_f	fuel flow
−1	p_3	compressor discharge pressure
−1	p_41	gas generator inlet pressure
−1	p_45	power turbine inlet pressure
−1	ps_fwd	forward primary servo
−1	ps_fwd-dot	forward primary servo rate
−1	ps_aft	aft primary servo
−1	ps_aft-dot	forward primary servo rate
−1	ps_lat	lateral primary servo
−1	ps_lat-dot	lateral primary servo rate
−1	ps_tr	tail rotor primary servo
−1	ps_tr-dot	tail rotor primary rate
−1	fp1c_p	ist cos delay aero nforc
−1	fp1s_p	ist sin delay aero nforc
−1	mf1c_p	ist cos aero flap moment
−1	mf1s_p	ist sin aero flap moment
−1	ml1c_p	ist cos aero lag moment
−1	ml1s_p	ist sin aero lag moment

[a] −1 implies state is linearized.

Acknowledgments

This research was conducted under Contract #26530 with NASA Ames Research Center, Moffett Field, California. The assistance by Dr. Mark B. Tischler of the Flight Controls and Cockpit Integration Branch (ARH) is obtaining the UH-60 simulation models used in this study is deeply appreciated.

References

[1]Garrad, W. L., and Eicher, L., "Eigenspace Design of Helicopter Flight Control Systems," U.S. Army Research Office, #DAAL03-86-0056, Research Triangle Park, NC, Nov. 1990.

[2]Horowitz, I. M., and Sidi, M., "Synthesis of Feedback Systems with Large Plant Ignorance for Prescribed Time Domain Tolerance," *International Journal of Control*, Vol. 16, No. 2, pp. 287–309.

[3]Houpis, C. H., "Technique for Designing Multivariable Control System," Air Force Wright Aeronautical Lab., AFWAL-TR-86-3107, Wright–Patterson AFB, OH, Jan. 1987.

[4]Horowitz, I., *Quantitative Feedback Theory (QFT)*, Vol. 1, QFT Publications, Boulder, CO, 1992, p. 30.

[5]Horowitz, I., "Survey of Quantitative Feedback Theory (QFT)," *International Journal of Control*, Vol. 53, No. 2, 1991, pp. 255–291.

[6]Horowitz, I., "Research in Advanced Flight Control Design," Air Force Wright Aeronautical Lab., AFFDL-TR-79-3120, Wright–Patterson AFB, OH, Jan. 1980.

[7]Cheng, R., "Rotorcraft Flight Control Design Using Quantitative Feedback Theory and Dynamic Crossfeeds," M.S. Thesis, Aeronautical Engineering Dept., California Polytechnic State Univ., San Luis Obispo, CA, Jan. 1995.

[8]Boje, E., and Nwokah, O. D. I., "Quantitative Feedback Design Using Forward Path Decoupling," *Proceedings of the Symposium on Quantitative Feedback Theory and Other Frequency Domain Methods*, Univ. of Strathclyde, Glasgow, Scotland, Aug. 1997, pp. 185–208.

[9]Kim, F. D., and Celi, R., "Simulation Modeling for Combat Rotorcraft Flight Control System Design," Joint Research Interchange, NCA 2-310, Univ. of Maryland, College Park, MD, June 1990.

[10]Hoh, R. H., and Mitchel, D. G., "Handling Qualities Specification—a Fundamental Requirement for the Flight Control System," *Advances in Aircraft Flight Control*, Taylor and Francis, Washington, DC, 1996, pp. 3–33.

[11]Yue, A., and Postlethwaite, I., "Improvement of Helicopter Handling Qualities Using H_∞ Optimisation," *IEEE Proceedings*, Vol. 137, Pt. D, No. 3, May 1990, p. 117.

[12]Hoh, R. H., Mitchell, D. G., Key, D. L., and Blanken, C. L., "Military Standard—Rotorcraft Flight and Ground Handling Qualities, General Requirements for US Army Aviation and Troop Command," MIL-STD, Nov. 1993 (draft).

[13]Landis, K. H., and Glusman, S. I., "Development of ADOCS Controllers and Control Laws," NASA CR-177339, 1985.

[14]Eitelbcrg, E., "Sampling Rate Design Based on (1-sT/2)," *International Journal of Control*, Vol. 48, No. 4, 1988, pp. 1423–1432.

[15]Berman, A., and Plemmons, R. J., *Nonnegative Matrices in the Mathematical Sciences*, Academic, New York, 1979, pp. 132–161.

[16]Nwokah, O. D. I., Nordgren, R. E., and Grewal, G. S., "Inverse Nyquist Array: A Quantitative Theory," *IEE Proceedings—Control Theory Applications*, Vol. 142, No. 1, 1995, pp. 23–30.

[17]Nwokah, O. D. I., and Perez, R., "On Multivariable Stability in the Gain Space," *Automatica*, Vol. 27, No. 6, 1991, pp. 975–983.

[18]Boje, E., "Non-Diagonal Controllers in MIMO Quantitative Feedback Design," *International Journal of Control* (submitted for publication).

[19]Lancaster, P., and Tismenetsky, M., *The Theory of Matrices*, 2nd ed., Academic, Orlando, FL, 1985, p. 154.

[20]Rosenbrock, H. H., *State Space and Multivariable Theory*, Wiley, New York, 1970, p. 7.

[21]Catapang, D., Tischler, M. B., and Biezad, D. J, "Robust Crossfeed Design for Hovering Rotorcraft," Symposium and Tutorial on Quantitative Feedback Theory, Aug. 1992, Dayton, OH, pp. 190–211.

[22]Borghesani, C., Chait, Y., and Yaniv, O., "Matlab® Quantitative Feedback Theory Toolbox," The Mathworks, Inc., Natick, MA, 1995, pp. 7–53.

[23]Key, D. L., "Handling Qualities Requirements for Military Rotorcraft," U.S. Army Aviation and Troop Command ADS-33D-PRF, St. Louis, MO, May 1996.

[24]Padfield, G. D., "Objective Assessment and Criteria Development," *Helicopter Flight Dynamics: The Theory and Application of Flying Qualities and Simulation Modelling*, AIAA Education Series, AIAA, Washington, DC, 1995, p. 366.